



Tensile acoustic rheometry for rapid and contactless characterization of soft viscoelastic biomaterials

Weiping Li^a, Eric C. Hobson^a, Kiera Downey^a, Timothy L. Hall^a, Jan P. Stegemann^a, Cheri X. Deng^{a,b,*}

^a Department of Biomedical Engineering, University of Michigan, Ann Arbor, MI, USA

^b Department of Mechanical Engineering, University of Michigan, Ann Arbor, MI, USA

ARTICLE INFO

Keywords:

Viscoelasticity
Biomaterials
Rheology
Tensile acoustic rheometry
Ultrasound

ABSTRACT

Accurately measuring the **viscoelastic properties of biomaterials** is critical for understanding their functions in biological systems and optimizing their development for specific applications. Conventional methods often require direct physical contact, which hinders longitudinal studies of sterile samples and impose strict requirements in sample preparation. Here, we introduce tensile acoustic rheometry (TAR), a technique for rapid, contactless characterization of soft viscoelastic biomaterials. TAR uses a dual-mode ultrasound approach to apply an upward force impulse, generating oscillatory tensile and compressive motion in a small, free-standing sample (~30 mm³) with its bottom immobilized on a pre-wetted flat surface by capillary stiction. High frequency ultrasound pulse echo detection is employed to track this motion via the movement of the top surface of the sample in real time. In this study, we developed a theoretical framework of the tensile-compression motion of the sample from which Young's modulus and viscosity of the sample are determined based on the TAR measurements. TAR was validated across a variety of samples, including engineered hydrogels and commercially available natural food products. Results from TAR measurements aligned closely with theoretical predictions, reported values, and shear wave elastography measurements. These findings underscore the versatility and flexibility of TAR as a robust, versatile rheological method for biomaterial characterization with minimal sample preparation requirements.

1. Introduction

Biological tissues respond to mechanical stimuli in ways dependent on both **elasticity (recoverable deformation)** and **viscosity (time-dependent deformation)** [1–4]. Engineered soft viscoelastic materials are used extensively in many fields including medicine, food science, and soft robotics [5–12]. For example, hydrogels composed of water-infused networks of hydrophilic polymer chains [5,8] are an important class of soft biomaterials that can model tissue ECM [7, 13–15], since the interactions between the liquid and solid phases in hydrogels [16] can recapitulate both the elastic and viscous components of the ECM as important effectors in controlling cell function [13,14]. Detailed understanding and quantitative characterization of soft materials are critical to provide insights for their applications [17,18].

However, accurate measurement of the viscoelastic properties of biological tissue samples *in vitro* and soft biomaterials remains challenging, often involving time-consuming and tedious processes.

Conventional tensile, compressive, indentation, and shear-based rheological techniques are generally low throughput and often requires direct physical contact with the samples. The risk of sample contamination and damage [19] makes these approaches not feasible for longitudinal characterization or monitoring of samples in sterile condition. Recent techniques such as microrheology have provided new capability of assessing local rheological properties at high spatial resolution by optically tracking the motion of dispersed probe particles within samples [20] including cell-laden hydrogels [21,22]. However, embedding exogenous tracers in samples may not always be feasible or desirable [20].

Here we report the development and validation of tensile acoustic rheometry (TAR) for mechanical characterization of soft viscoelastic materials using a dual-mode ultrasound technique, to generate and detect the tensile-compression movement of a free-standing sample without direct physical contact. A theoretical framework of the tensile-compression motion of the sample was developed to allow for the

* Corresponding author. Department of Biomedical Engineering, University of Michigan, Ann Arbor, MI, USA.

E-mail address: cxdeng@umich.edu (C.X. Deng).

<https://doi.org/10.1016/j.biomaterials.2025.123325>

Received 25 November 2024; Received in revised form 11 February 2025; Accepted 6 April 2025

Available online 8 April 2025

0142-9612/© 2025 Elsevier Ltd. All rights are reserved, including those for text and data mining, AI training, and similar technologies.

determination of Young's modulus and viscosity based on TAR measurements. TAR was validated across a variety of samples, including engineered hydrogels and natural food samples. These results demonstrate TAR as a robust approach for viscoelastic characterization requiring minimal sample preparation.

2. Materials and methods

2.1. Cell culture

Normal human lung fibroblast cells (NHLF) (Lonza Inc., Walkersville, MD) were cultured in Dulbecco's-modified eagle medium (DMEM) supplemented with 10 % FBS and 1 % penicillin streptomycin. Human umbilical vein endothelial cells (HUVEC) were isolated from umbilical cords from the University of Michigan Mott Children's Hospital [23]. HUVECs were plated in tissue culture flask and grown in fully supplemented Vasculife endothelial cell culture medium (Lifeline Cell Technology, Frederick, MD). Human bone marrow-derived mesenchymal stromal cells (MSC; RoosterBio, Inc.) were maintained in MSC growth medium (Lonza). Cells were maintained at 37 °C in 100 % humidified air with 5 % CO₂. Medium was changed every other day.

2.2. Cell – free agarose and gelatin samples

A 20.0 mg/ml (2 %) agarose stock solution was prepared by dissolving agarose powder (Type 1-A; Sigma) into PBS with continuous heating and stirring. The solution was transferred to a 50 °C water bath and was diluted with pre-heated PBS to generate additional solutions at concentrations of 5.0 mg/ml (0.5 %) and 10.0 mg/ml (1 %). The solutions were placed in a 3d-printed container filled to three heights (4, 6 and 8 mm), and placed at room temperature for 1 h to solidify. A 100 mg/ml (10 %) gelatin stock solution was prepared by dissolving bovine gelatin powder (200 Bloom, 30 mesh; Gelatin Innovations) into PBS with continuous heating and stirring. The solution was diluted with pre-heated PBS to generate solutions of 50 mg/ml (5 %) and 75 mg/ml (7.5 %) gelatin concentrations. The solutions were placed in a 3D-printed container with filled to three heights (4, 6 and 8 mm), and placed at room temperature for 1 h to solidify. Round and square punches (diameter 4, 6 and 8 mm) were used to create cylindrically and rectangular-shaped samples with different diameters from the solidified samples for TAR tests.

2.3. Fibrin gel with HUVECs and NHLFs

Fibrinogen (Sigma-Aldrich, St. Louis, MO) was dissolved in phosphate-buffered saline (PBS) at 37 °C (12.8 mg/mL active clottable protein), and then sterile filtered through a 0.22- μ m syringe filter (Millipore Sigma) and kept on ice until ready for use. One ml cell-laden gels were made by mixing fibrinogen 625 μ l fibrinogen, 20 μ l thrombin (Sigma, 50 Unit/ml), 255 μ l DMEM, 100 μ l FBS and 250k or 500k cells, respectively. The well mixed cell-fibrinogen suspension was quickly placed in a 24-well plate. After dispensing the hydrogel solution, the 24-well plates were incubated at 37 °C for 30 min for gelation. A punch (diameter 8 mm) was used to create a disk-shaped sample. Fibrin gel with cells were incubated in fully supplemented Vasculife medium at 37 °C with 100 % humidified air containing 5 % CO₂, and the medium was changed every other day.

2.4. Collagen gels with and without MSCs

Collagen type I (MP Biomedicals, Solon, OH) stock solution was prepared at 4.0 mg/ml in 0.02 N acetic acid. 500 μ l Collagen hydrogels (final concentration as 2.0 mg/ml) were made by mixing 150 μ l DMEM, 50 μ l FBS, 50 μ l NaOH (Sigma Aldrich) and 250 μ l of 4 mg/ml collagen type I stock solution. One ml cell-laden gels were made by mixing the collagen solution with 250 k or 500k MSCs, respectively. The mixture

was pipetted into 48-wells plate and incubated at 37 °C for 30 min to solidify the mixture. After gelation, hydrogels were moved to 24-well plates and a punch (diameter 8 mm) was used to prepare a disk sample for experiments. The samples were then incubated in MSC growth medium at 37 °C and 5 % CO₂. After 24 h, the media was changed to osteogenic media (Lonza) and the media was then changed every other day. Cell-free collagen gels were made in a similar way without addition of MSCs.

2.5. Food samples

Natural food samples were purchased from local supermarkets including Jello (Mango Flavor Pudding), soft and firm Tofu (House Food), chicken breast (Kirkland), and cooked pork blood (Asian Market). The food samples were cut into cylinders using a punch (diameter 6 mm).

2.6. TAR setup

For TAR testing, a sample, typically in the shape of a cylinder was placed on a flat smooth surface, e.g., a microscope glass slide, a standard cell culture dish, or a microplate. The sample was free standing except its bottom surface, which was immobilized on the supporting surface by capillary stiction provided by a thin liquid layer between the sample bottom and the supporting surface.

TAR utilizes a composite ultrasound transducer assembly consisting of two concentric, co-linearly aligned focused ultrasound transducers. The outer annular transducer (center frequency 1.5 MHz) was used as the excitation transducer and the inner transducer (center frequency 7 MHz) worked as the detection transducer. The ultrasound transducer assembly was placed beneath the sample and submerged in a water bath, which provided acoustic coupling for the transducers and the bottom of the supporting plate for the sample. The transducers were directed upward and aimed at the center or another designated location of the top surface of a sample. A 3D motion control platform (Velmex) was used for alignment and positioning of transducers. The excitation transducer was driven by a power amplifier (75A250; Amplifier Research) and a waveform generator (33220A; Agilent) to induce motion in the sample. The detection transducer was controlled by a pulser/receiver (5900 PR; Olympus) to operate in a pulse-echo mode to detect reflection signals from the sample surface, which was digitized with a model 5443 Pico-scope (Pico Technology, St Neots, UK). The excitation and detection transducer were synchronized using a pulse generator (Model 565; BNC) for excitation and tracking of sample surface movement.

2.7. TAR measurement of displacement of top surface of a free standing sample

In TAR, the excitation transducer generates a short excitation pulse (duration 33 μ s, acoustic pressure 2.5 MPa) that travels through the sample from bottom to top and produces an upward impulse of force, in the form of the acoustic radiation force, on the top surface of the sample. This force impulse induces a tensile extension of the sample with its bottom fixed on the supporting surface, followed by a tensile/compression oscillatory motion, which is detected by the detection transducer via the movement of the top sample surface using pulse-echo detection at a high pulse repetition frequency (PRF) of 5 KHz, based on the traveling time of the detection pulse to and from the sample surface. Specifically, to determine the surface movement from the echo signals, a short time window was placed around the surface reflection signal and the phase of the Fourier transform calculated over this time window at the frequency of maximum energy was used to calculate a relative displacement compared to pre-excitation. The MATLAB Phase Unwrap command was used across sequential phase measurements to allow for accurate displacement measurements beyond a single acoustic cycle (approximately 214 μ m) as long as the max velocity was less than one

half cycle per imaging pulse period (approximately 0.5 m/s). A second Fourier transform of the resulting surface displacement data was performed to obtain the power spectrum of the surface movement, from which the peak frequency and half-width-at-half maximum (HWHM) were determined and used to calculate the shear modulus and viscosity of the sample using a lumped model of the tensile/compressional movement of the sample as described in supplemental information (SI).

2.8. Shear wave elastography

Shear wave elastography (SWE) was performed to obtain an independent measure of elastic modulus E of the samples in our TAR experiments using a Logiq E10 imager (GE Healthcare) in elastography mode with an L8-18i probe at 14 MHz. For shear wave imaging, the sample was immersed in phosphate buffered saline (PBS) in a tissue culture dish or a microplate. The probe, secured using a custom-made holder, was placed on the bottom of the dish/microplate coupled with ultrasound gel. A region of interest (ROI) was defined in the middle of the sample to ensure elastography measurements to minimize boundary effects. SWE measurements were then taken from a 0.5 mm^2 rectangular ROI at the center of the gel sample. The depth of the ROI from the bottom of the plate was kept the same for all measurements. For each sample, five replicate measurements were taken and averaged to obtain the elastic modulus.

2.9. Finite element analysis (FEA) modeling of TAR using COMSOL

A COMSOL model was constructed to simulate the behavior of samples during TAR. A 2D axisymmetric model was created for the cylindrical geometry of a sample used in TAR. The Structural Mechanics module was used to model the sample as a linear viscoelastic material with fixed boundaries on the bottom and a free boundary condition on other surfaces including the top surface. The parameters used in the simulation include sample dimension, Young's modulus, and viscosity, were based on the values from TAR experiments. The model was used to simulate the response of the sample to ultrasound excitation and determine the surface displacement at the center of the sample, which was measured in TAR.

2.10. Statistical analysis

All experiments were repeated for at least three different samples. For data complying with the normal distribution, two-sample t -test is applied. Nonparametric Mann-Whitney test is performed for the data which doesn't follow a normal distribution. A p -value < 0.05 was considered statistically significant.

3. Results

3.1. Theoretical framework of the oscillatory tensile-compression motion of a free-standing sample immobilized by capillary stiction

TAR is optimized for testing small-volume samples, e.g., cylindrical in shape (e.g., $\sim 3 \text{ mm}$ radius and $\sim 5 \text{ mm}$ height), placed on a flat surface that is pre-wetted with a small drop of liquid. For engineered samples typically stored in a cell culture dish or microplate with medium or PBS, the liquid was briefly removed for a few seconds during the TAR measurement which lasted a few seconds. The small amount of liquid formed a thin layer, or a disk-like plug (with radius R and thickness h), between the bottom of the sample and the supporting surface (Fig. 1a). Due to the effects of surface tension, a capillary stiction force [24,25] is generated, $F_s = \pi R^2 \left(\frac{\sigma \cos \theta_1}{h} + \frac{\sigma \cos \theta_2}{h} - \frac{1}{R} \right)$, that holds the sample in place on the supporting surface. Here σ represents the surface tension, θ_1 and θ_2 are the contact angle of the liquid plug with the support surface and bottom surface of the sample, respectively. The capillary stiction force immobilizes the bottom of the sample (mass m) on the supporting surface. Thus to lift the sample off the surface, an external upward force is required to overcome both the capillary stiction and the gravitational force (mg). The minimal separation force is given by Refs. [24,25] $F_{min} = F_s + mg$. As an example, assuming $R \gg h$ and $\theta_1 = \theta_2 = 0$ (perfectly wetted surfaces), $\sigma = 0.035 \text{ Nm}^{-1}$ (for cell culture medium), and $h = 0.1 \text{ mm}$, the lower bound of F_{min} for our experiments can be estimated to be 3.7 N , which is several orders of magnitude greater than the gravitational force of a typical sample in our study.

If the free-standing sample is subjected to an upward impulse force less than F_{min} , the bottom of the sample remains firmly grounded on the supporting surface. However, if a short upward force impulse is applied to the sample with a fixed bottom, the sample sustains an initial upward tensile stretch, resulting in a tensile strain and stress distribution within the continuum of the sample. Notably, the deformed sample will then undergo elastic recovery from the initial stretch, followed by a damped oscillatory tensile-compressive motion driven by the interplay of inertia, elastic restoring forces, and the sample's viscosity.

For a homogeneous, isotropic, free-standing sample with a fixed bottom (cross section A , thickness or height L_0 , mass m , density ρ , Young's modulus E , and dynamic viscosity η), its vertical oscillatory tensile-compressive motion can be regarded as one-dimensional (1D) to first order approximation. Assuming linear elasticity, the total restoring force F in the deformed sample is related to the total deformation Δl as $\frac{F}{A} = -E \frac{\Delta l}{L_0}$, or equivalently, $F = -\frac{EA}{L_0} \Delta l = -k_{eq} \Delta l$, where $k_{eq} = \frac{EA}{L_0}$ is the equivalent spring constant. This relationship reveals a Hookean behavior of the tensile-compression motion of the sample, which can be regarded as a mass-spring system. As detailed in the **Supplemental Information (SI)**, the equivalent mass of this mass-spring system is derived as $m_{eq} = \frac{1}{3}m$, assuming a linearly varying velocity profile along the vertical axis of the sample from the fixed bottom to the free top surface. The equivalent damping constant is derived as $\gamma_{eq} = \frac{A\eta}{L_0}$,

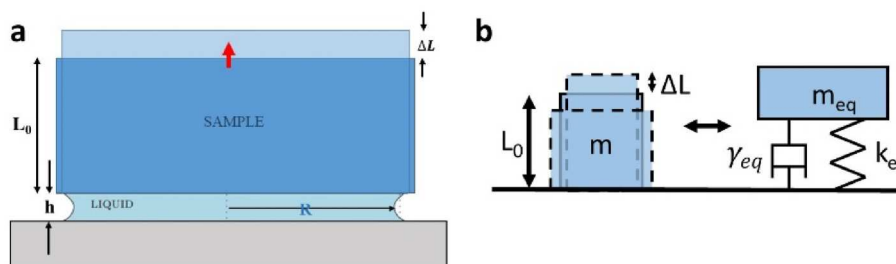


Fig. 1. a. A sample of a cylindrical shape (radius a , thickness L_0) placed on a flat surface is immobilized by capillary stiction due to a liquid plug (height h , radius R). b. Equivalent model of tensile/compression motion of the sample as a damped mass-spring system.

considering the viscous energy dissipation caused by the velocity gradient or relative motion within the sample. Thus the tensile-compressive motion of the sample can be modeled as a damped mass-spring system (Figs. 1b and SI) with a damping coefficient $\Gamma = \frac{\gamma_{eq}}{2m_{eq}} = \frac{3\eta}{2\rho L_0^2}$ and intrinsic resonant frequency $\omega_0 = \sqrt{\frac{k_{eq}}{m_{eq}}} = \frac{1}{L_0} \sqrt{\frac{3E}{\rho}}$, respectively. Since Γ corresponds to the half frequency width at half maximum (HWHM) of the resonant frequency ω_T , i.e., $\Gamma = \frac{\Delta\omega}{2}$, the viscosity and Young's modulus can be obtained respectively as

$$\eta = \frac{2\rho L_0^2}{3} \Gamma = \frac{2\rho L_0^2}{3} \frac{\Delta\omega}{2}, \quad (1)$$

and

$$E = \frac{\rho L_0^2}{3} (\omega_T^2 + \Gamma^2) = \frac{\rho L_0^2}{3} \left(\omega_T^2 + \frac{\Delta\omega^2}{4} \right). \quad (2)$$

3.2. TAR generates and detects tensile-compressional motion in a free-standing sample

In TAR, a dual-mode ultrasound technique is employed to induce and detect the oscillatory tensile-compressional motion of a free-standing sample. As shown by the example in Fig. 2a, a short excitation ultrasound pulse (duration $\sim 33 \mu\text{s}$) was applied from below, targeting the top surface of a cylindrical 5% gelatin sample (radius $a = 2.8 \text{ mm}$, height L_0). The excitation ultrasound pulse generated an upward impulse force in the form of the acoustic radiation force (ARF), or F_{ARP} , acting predominantly on the top surface of the sample. Assuming a plane wavefront and perfect reflection at the air-sample interface, F_{ARP} depends on the acoustic intensity of the excitation pulse I and is estimated as $F_{ARP} = \pi r_d^2 \frac{2I}{c}$, where c is the speed of sound in the sample material [26, 27], and r_d is the half-width of the ultrasound beam at the focal point on the sample surface. For the excitation pulse used in this study ($I = 1.33 \times 10^6 \text{ W}\cdot\text{m}^{-2}$ and $r_d \approx 0.1 \times 10^{-3} \text{ m}$), $F_{ARP} \approx 6.0 \times 10^{-3} \text{ N}$, which is significantly less than the lower bound of the capillary stiction force estimated in this study. Consequently, the bottom of the sample remained firmly grounded on the supporting surface during TAR, while

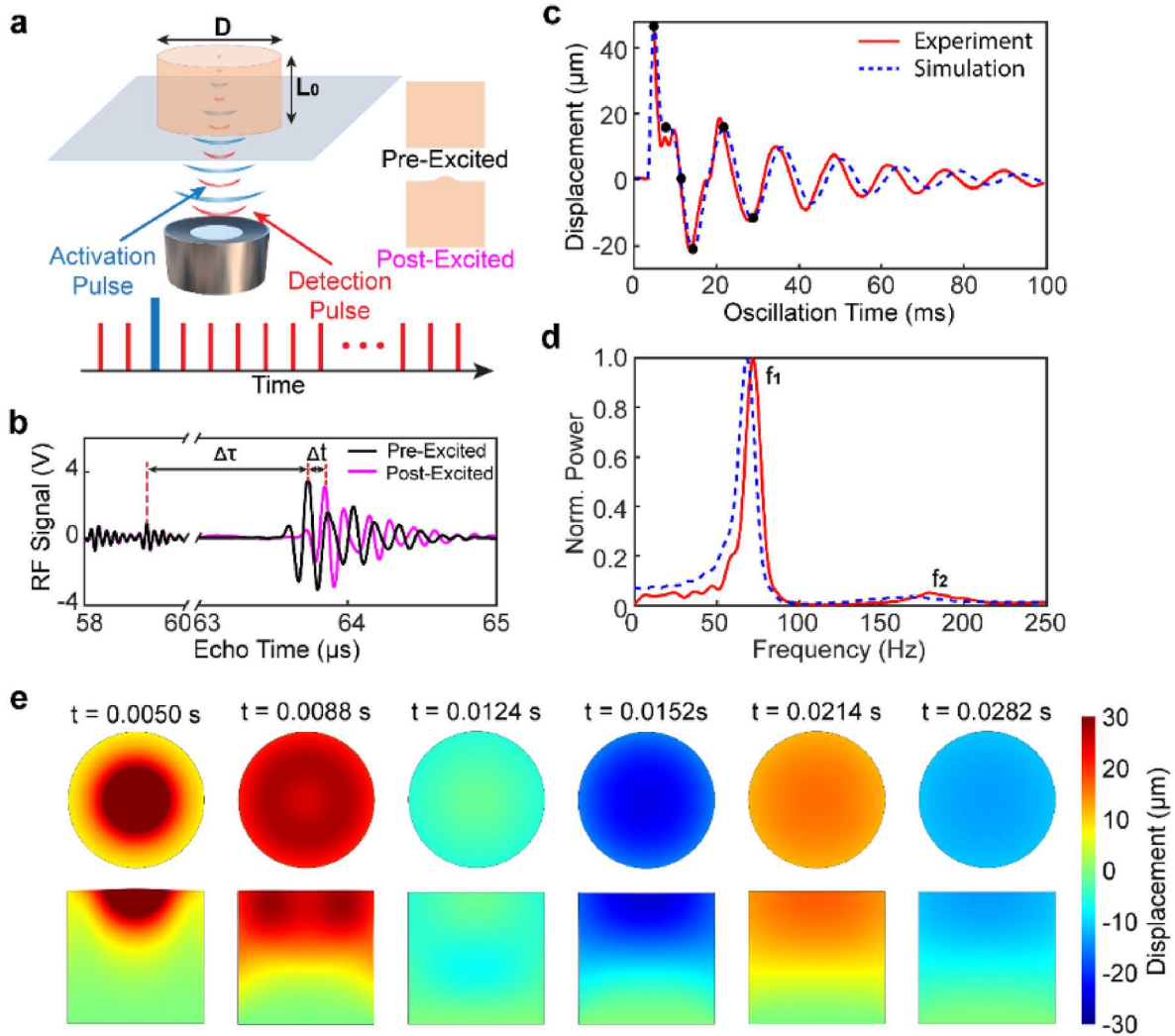


Fig. 2. a. Schematics of TAR. An excitation ultrasound pulse generates tensile/compression motion of a cylindrical shaped sample (diameter D , thickness L_0) detected using pulse-echo detection via the movement at the center of the top surface of the sample. Inset: surface deformation induced by the excitation ultrasound pulse. b. Backscattered signals from the sample surface before and after excitation, with a temporal shift Δt due to change in travel distance of the detection pulse to/from sample surface. c. Surface displacement measured using TAR compared with COMSOL simulation. d. Normalized power spectra of surface displacement with frequency peaks at $f_1 = 72.05 \text{ Hz}$ and $f_2 = 178 \text{ Hz}$ from TAR measurements, as well as $f_1' = 68.5 \text{ Hz}$, and $f_2' = 168 \text{ Hz}$ from COMSOL simulation. e. Displacement distribution on the sample surface (top) and within the sample (bottom) in the central transverse plane.

f_{ARP} induced an upward tensile stretch of the sample as described in the previous section of theoretical framework of TAR. The subsequent tensile-compressional motion, driven by the interplay of inertia, elastic restoring force, and viscosity, essentially represents the impulse response of the sample with a fixed bottom surface that is modeled as a damped mass-spring system (SI).

In TAR, high-sensitivity pulse-echo ultrasound detection at a high pulse repetition frequency (PRF, e.g., 5 KHz), is used to detect the oscillatory tensile-compressive motion of the sample by tracking the sample's top surface displacement in real time based on the temporal shifts in the echo signal from the air-sample interface (Fig. 2b). Initially, the height of the sample was determined using pulse-echo detection as $L_0 = 5.43 \text{ mm}$, representing the equilibrium position before the application of the excitation pulse. After excitation, TAR detected the damped harmonic motion of the sample's surface (Fig. 2c). The power spectrum of this motion exhibited a frequency peak at $f_1 = 72.1 \text{ Hz}$ with a full width at half maximum (FWHM) $\Delta f_1 \approx 10.2 \text{ Hz}$ (Fig. 2d). From this, the damping coefficient was determined as $\Gamma = \frac{\Delta\omega}{2} = \pi\Delta f_1 \approx 16.0 \text{ rad} \cdot \text{s}^{-1}$, and the Young's modulus as $E = \frac{(2\pi f_1 L_0)^2 \rho}{3} = 2.12 \text{ kPa}$ and the dynamic viscosity $\eta = \frac{2\rho L_0^2 \Gamma}{3} = 0.33 \text{ Pa}\cdot\text{s}$, using Eq. (1) and Eq. (2) and assuming $\rho = 1050 \text{ kgm}^{-3}$. These values are consistent with reported measurements for 5% gelatin [28,29]. Notably, real time measurements of the damped surface displacement, which lasted about 0.1 s–0.2 s in a typical samples in TAR, enabled the determination of Young's modulus and viscosity within a fraction of a second.

COMSOL simulations were performed to model the dynamic behavior of the sample subjected to the excitation pulse, using the Young's modulus and viscosity values measured in TAR (SI). The simulated surface displacement and corresponding power spectrum agree closely with experimental TAR results (Fig. 2c and d). The simulation also revealed an initial non-uniform surface displacement caused by the focused ultrasound beam, which transitioned to uniform displacement within 0.015 s (top, Fig. 2e; Supplemental Video 1), after which 1D tensile-compressional oscillatory motion dominated (bottom, Fig. 2e–Supplemental Video 2). These results suggest that the initial force impulse generated a surface wave (Rayleigh wave, RW), which rapidly decayed while the 1D tensile-compressional motion persisted longer. The power spectrum confirmed this interpretation, with a secondary peak at $f_2 = 178 \text{ Hz}$ potentially corresponding to a resonant mode of RW [28,30,31], consistent with previous findings in resonant acoustic rheometry (RAR) [28,30]. The angular frequency of RWs is related to the shear modulus G of the material and the wavenumber of the surface wave k as $\omega_{RW} = \sqrt{\frac{Gk^2}{\rho}}$. For TAR, assuming a free boundary condition at $r = a$, the $(0, 1)$ mode satisfies $J_0(ka) = 0$, resulting in $ka = 3.832$. From this, the shear modulus was determined to be $G = \frac{\rho\omega_{RW}^2}{k^2} = \frac{4\pi^2\rho f_{RW}^2 a^2}{(ka)^2} = 0.70 \text{ kPa}$ for $f_{RW} = f_2 = 178 \text{ Hz}$. Assuming the material was incompressible (Poisson ratio $\nu \approx 0.5$), the Young's modulus was calculated as $E = 3G = 2.1 \text{ kPa}$, in agreement with the value derived from $f_1 = 72.05 \text{ Hz}$.

The viscosity of the sample was determined from the HWHM at f_2 [28,30] using the damping coefficient of RW, $\Gamma_{RW} \approx \frac{0.45\pi k^2}{\rho} = \pi\Delta f_2$. Although Δf_2 was challenging to measure due to the low amplitude at f_2 (Fig. 2d), the large ratio of the RW damping coefficients to the tensile-compression damping coefficient ($\frac{\Gamma_{RW}}{\Gamma} = 0.3(ka)^2 \frac{L_0^2}{a^2} \approx 16.7$) is consistent with the broader peak width at f_2 compared to f_1 , indicating significantly higher damping for RW than for tensile-compression motion.

While TAR is applicable for characterization of solid samples and RAR can characterize both viscoelastic liquid and viscoelastic solids, the consistent results shown in this example provided valuable validation of TAR against RAR measurements of the same sample.

3.3. TAR measurements of viscoelasticity are independent of sample diameter

We conducted a systematic comparison of the lumped mass-spring model and COMSOL finite element analysis (FEA) simulations to evaluate the effects of various parameters on the frequency spectrum, and thereby the determination of the viscosity and Young's modulus (Eqs. 1 and 2). Overall, the COMSOL simulations and the lumped mass-spring model produced consistent results. Specifically, the peak frequency of the motion at the center of the sample surface was independent of the sample diameter (Fig. 3a) and inversely proportional to the sample thickness (Fig. 3b), as described by the relationship $f_1 = \frac{1}{2\pi L_0} \sqrt{\frac{3E}{\rho}}$, derived from the mass-spring model. Since TAR directly measures the sample thickness, these results highlight the versatility and simplicity of determining Young's modulus using TAR for samples with varied dimensions.

While similar trends for the HWHM vs. sample thickness were observed, COMSOL simulations predicted slightly higher values than the damped mass-spring model (theory, Fig. 3c). Importantly, consistent results were obtained from both COMSOL simulations and the damped mass-spring model across samples with varying Young's modulus (Fig. 3d) and viscosity (Fig. 3e). Higher HWHM values were observed in samples with smaller thickness, which corresponded to higher frequencies of tensile-compression motion (Fig. 3f). Additionally, larger discrepancies between COMSOL simulations and mass-spring model predictions were noted in samples with lower viscosity (Fig. 3f). These differences suggest that energy dissipation mechanisms modeled in COMSOL for a continuum, such as those associated with 3D movements within the sample beyond vertical motion, are not fully captured by the mass-spring model. Similarly, approximation in the mass-spring system, such as the assumption of a linear velocity profile, may contribute to these discrepancies.

Taken together, these results validate and highlight the strength of TAR and the lumped mass-spring model for the rapid viscoelastic characterization of samples based on measurements of sample surface movement.

3.4. TAR provides rapid and robust measurements of viscoelastic properties

We conducted a series of experiments to evaluate TAR in samples of varying dimensions and properties. For cylindrical gelatin samples, TAR measurements demonstrated excellent agreement with predictions from the mass-spring model for the frequency of the surface motion across different sample diameters (Fig. 4a) and thicknesses (Fig. 4b). The Young's modulus (Fig. 4c) and viscosity (Fig. 4d) determined from TAR measurements showed that samples with higher gelatin concentrations were stiffer and more viscous, consistent with reported measurements [28]. Similarly, TAR measurements for cylindrical agarose samples aligned well with mass mass-spring model predictions for frequency, Young's modulus and viscosity as functions of sample dimensions and agarose concentrations (Fig. 4e–h). While the viscosity of agarose samples was comparable to that of gelatin samples, their Young's modulus was significantly higher, reflecting their greater stiffness. These results not only align with previously reported values [28] but also highlight TAR's capability to measure a wide range of elasticity values, demonstrating its versatility for viscoelastic characterization.

We conducted additional TAR experiments with the ultrasound excitation and pulse-echo detection positioned at off-center locations on the sample surface. The results indicated that TAR measurements of surface displacement (Figs. S1a and S1b), as well as the derived Young's modulus and viscosity of the samples (Figs. S1c and S1d) were unaffected by the off-center excitation and detection. These findings were consistent with the lumped mass-spring model of the tensile-compressional motion during TAR, demonstrating that the

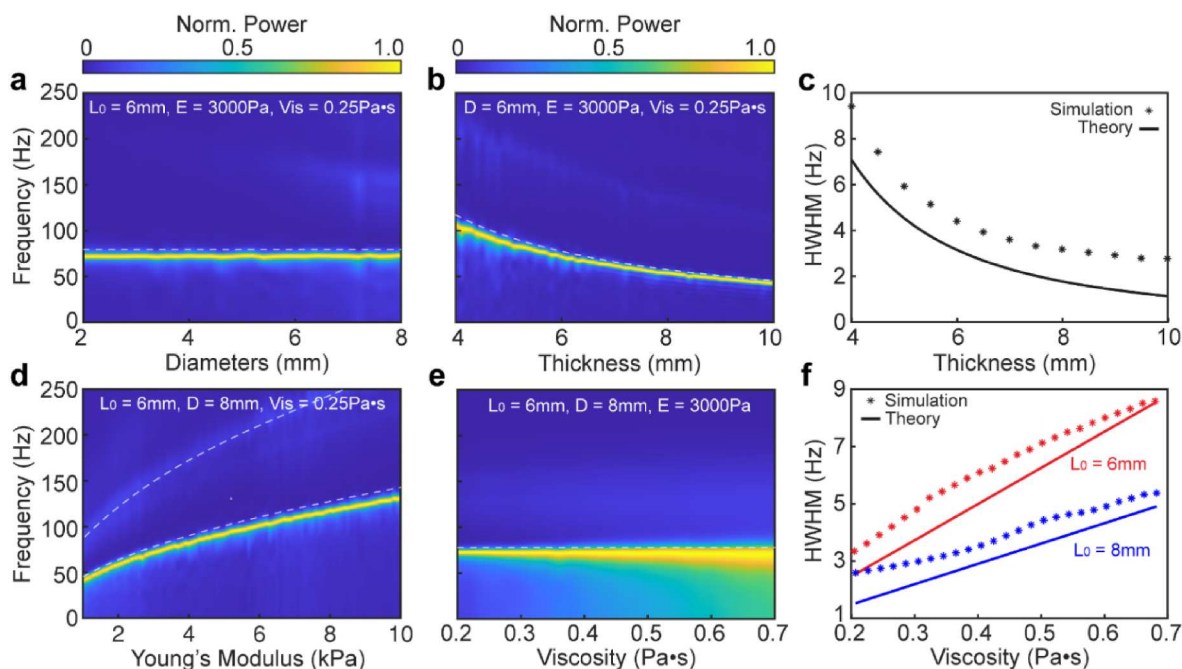


Fig. 3. Normalized power spectra of surface movement from COMSOL simulation and mass-spring model (dashed line) vs. diameter D (a) and thickness L_0 (b). c. COMSOL and mass-spring model prediction (theory) of half width half maximum (HWHM) of the surface movement vs. thickness. Normalized power spectra of surface movement from COMSOL simulation and mass-spring model (dashed line) vs. Young's modulus (d) and viscosity (e). f. COMSOL and mass-spring model prediction (theory) of HWHM of the surface movement vs. viscosity in samples with two diameters when $E = 3000$ Pa.

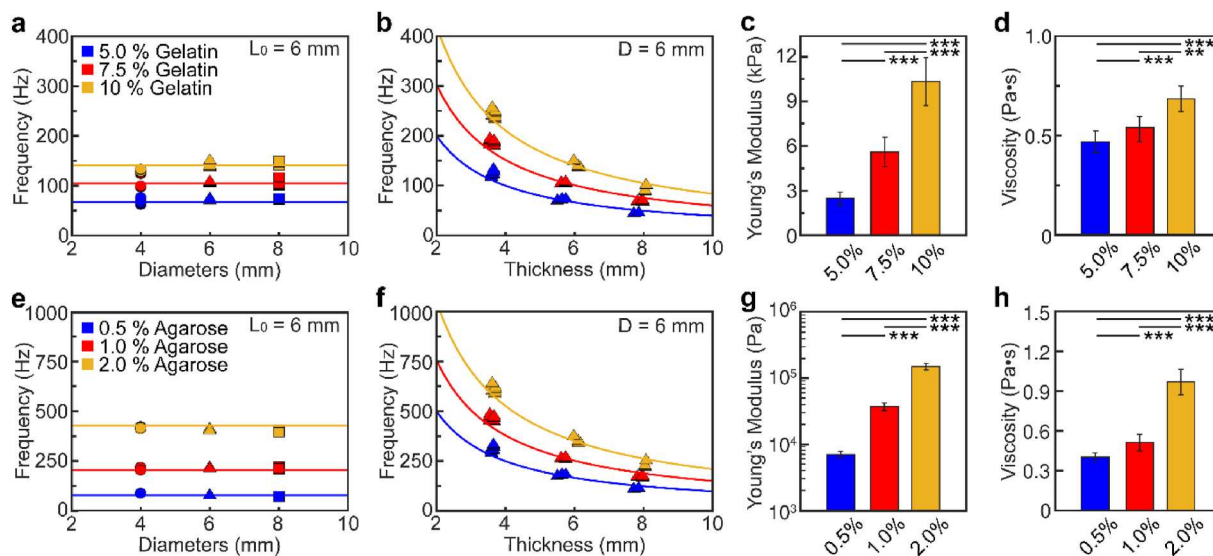


Fig. 4. Comparison of TAR measurements (symbols) and mass-spring model prediction (solid lines) for 5 %, 7.5 %, and 10 % gelatin samples in terms of frequency of surface movement vs. sample diameter (a) and thickness (b). Young's modulus (c) and viscosity (d) determined from TAR experiments in samples (Diameter 6 mm, thickness 6 mm) with 5 %, 7.5 %, and 10 % gelatin respectively. $n = 18$ for all groups. Comparison of TAR measurements (symbols) and mass-spring model prediction (solid lines) 0.5 %, 1.0 %, and 2.0 % agarose samples respectively in terms of frequency of surface movement vs. sample diameter (e) and thickness (f). Young's modulus (g) and viscosity (h) determined from TAR experiments in samples (Diameter 6 mm, thickness 6 mm) with 0.5 %, 1.0 %, and 2.0 % agarose respectively. $n = 15$ for all groups.

measurements are independent of the location of the applied forces on the sample surface. This underscores the validity of the 1D approximation and robustness of TAR.

TAR measurements using samples with a square surface also exhibited a consistent dominant frequency of surface displacement. While additional components were observed (Fig. S2a), they were present at much lower intensity levels (Fig. S2b). The Young's modulus measurements were unaffected by the shape of the sample surface, but

viscosity measurements showed greater variability, particularly for larger square samples. This suggests that different modes of movement influence the energy distribution at the primary frequency peak, which was used to estimate viscosity.

3.5. TAR measurements of Young's modulus compared with shear wave elastography

Shear wave elastography (SWE) is an ultrasound imaging technique used to assess the elasticity of soft tissues *in vivo* by measuring the shear wave velocity $V_s = \sqrt{\frac{G}{\rho}}$, where G is the shear modulus and ρ is the density of the tissue [32]. SWE has proven to be a valuable tool for diagnosing and monitoring diseases such as malignant breast lesions, liver fibrosis, and thyroid nodules [32]. In this study, we conducted paired experiments on the same samples using SWE and TAR to compare their measurements of Young's modulus across a wide range of materials, including engineered hydrogels (Fig. 5a) and commercially purchased food samples of various sizes (Fig. 5b). For the food samples tested using both TAR and SWE, we also tested SWE in larger samples (SWE_L, Fig. 5b) to examine whether the small size affected measurements based on propagating shear wave in SWE. The values of Young's modulus measured using TAR are slightly higher than those obtained with SWE in both small and larger sized samples, with differences within 10–15 %, which may be attributed to the irregularities in manual sample preparation for TAR. Despite these minor discrepancies, the strong general agreement between TAR and SWE validates the reliability of TAR and provides a useful reference for SWE measurements in complex *in vivo* environments.

3.6. Longitudinal measurements of Young's modulus of cell-laden hydrogels using TAR

We evaluated the utility of TAR for longitudinal assessment of cell-laden hydrogels under sterile condition to monitor changes in their mechanical properties over time. These samples were kept in incubators in sterile condition and were taken out for less than 1 min for TAR measurements when medium was removed for several second for non-contact TAR measurements. After TAR, fresh medium was added and samples were placed into incubator until the next TAR measurement. Experiments were conducted on fibrin gels embedded with normal human lung fibroblasts (NHLFs) to detect changes in stiffness of the same samples over time. Compared to cell-free fibrin gel samples, which maintained constant thickness, cell-laden samples showed cell proliferation (Fig. S3a) and significant reduction in thickness dependent on cell seeding density, as indicated by the travel time of the echo signals from the sample surface (Fig. S3b). Samples with a cell seeding density of 1 million cells/ml underwent severe compaction, with thickness decreasing to less than 300 μm within two days of culture, at which point TAR measurements were no longer feasible (Fig. S3b). Additionally, TAR measurements showed that the Young's modulus of cell-laden

samples decreased over time, with greater reductions observed at higher cell seeding densities, while the cell-free gels remained mechanically unchanged (Fig. S3c).

In comparison, fibrin gels embedded with both NHLFs and HUVECs at a 1:1 ratio showed much less thickness reduction (less than 25 %) over 14 days. Concurrently, vessel-like structures formed within the constructs (top, Fig. 6a), and the Young's modulus measured in the same samples decreased gradually over time. This softening effect was more pronounced in samples with higher cell seeding densities (bottom, Fig. 6a). We further tested TAR on collagen samples embedded with mesenchymal stem cells (MSCs) cultured in osteogenic differentiation medium (top, Fig. 6b). Cell proliferation was observed visually in these samples (top, Fig. 6b). The Young's modulus of the collagen constructs began to increase around day 3, with larger increases detected in samples with higher cell densities (bottom, Fig. 6b). These results reveal the impact of different cells on the mechanical properties of the hydrogel-based constructs.

4. Discussion

4.1. Different mechanisms and applicability of TAR and RAR for viscoelastic characterization

We have previously reported the use of RAR, which also employs a dual-mode ultrasound technique, for non-contact characterization of both viscoelastic liquid and soft materials housed in standard 96- or 48 well microplates [28,30]. While both TAR and RAR provide rapid ultrasound-based characterization of soft biomaterials, the techniques differ in their underlying physical principles and suitability for specific applications.

In RAR, the samples are housed in a sample chamber, e.g. a well of a 96-well microplate, thus the samples are restricted in all boundaries except the top surface. For these samples, application of an excitation ultrasound generates resonant modes of surface waves in the samples, which can be either liquid or solid, and can monitor phase transitions and the changes in viscoelastic properties in real time. Specifically, RAR determines viscoelastic properties using the specific dispersion relation of surface waves, which depends on parameters such as surface tension (for liquids), shear modulus (for solids), and viscosity. Because RAR relies on the formation of resonant surface wave, it is most effective for testing confined samples with fixed boundary conditions and a free surface. This makes RAR particularly suited for studying dynamically evolving biomaterials, such as during coagulation or polymerization/gelation processes. However, RAR is less applicable for pre-formed samples with irregular shapes that lack confined boundaries.

In contrast, TAR is suited for characterizing free-standing samples

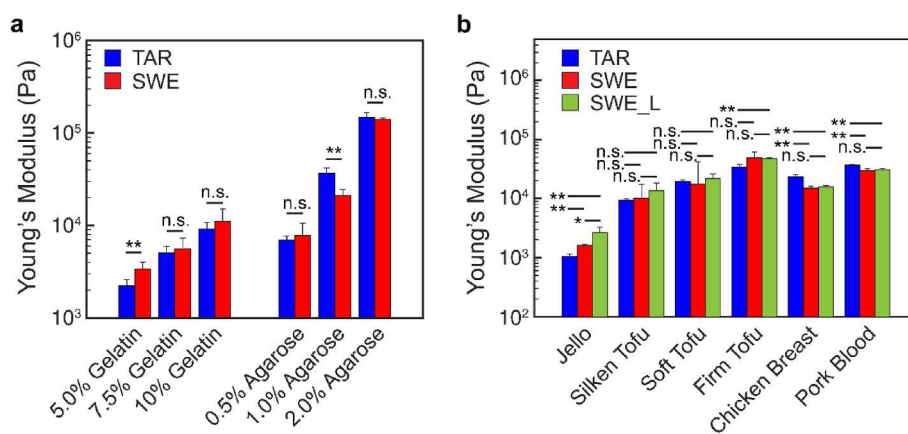


Fig. 5. a. Measurements of the Young's modulus of the same gelatin and agarose samples using TAR and SWE. $n = 15$ for all groups. b. Measurements of Young's modulus of the same food samples using TAR and SWE as well as Young's modulus measured using larger food samples (SWE_L). Results are presented as mean \pm standard deviation. $n = 3$ for all groups. n.s.: not significant; *: statistical difference as $p < 0.05$.

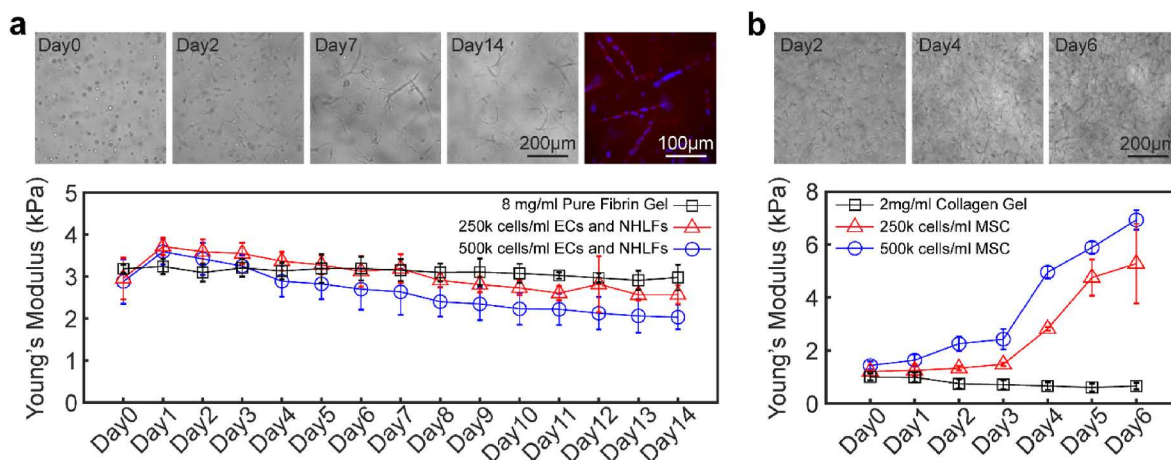


Fig. 6. Longitudinal TAR measurements of Young's modulus of the same samples at different time points. **a.** Top: Bright field images of a fibrin gel (8 mg/ml) embedded with normal human lung fibroblasts (NHLFs) and HUVECs at 1:1 ratio with total cell density of 500 k cells/ml. Samples were stained with DAPI (blue) and UEA-I (red) on day 14. Bottom: Measured Young's modulus of cell-free fibrin gels, fibrin gels with NHLFs and HUVECs at 250 k cells/ml and 500 k cells/ml respectively. $n = 8$ for all groups. **b.** Top: Collagen gels embedded with mesenchymal stem cells (MSCs) at 500 k cells/ml in osteogenic medium. Bottom: Measured Young's modulus of cell-free collagen gels, collagen gels with MSCs at 250 k cells/ml and 500 k cells/ml in osteogenic medium respectively. (For interpretation of the references to colour in this figure legend, the reader is referred to the Web version of this article.)

without stringent restrictions on sample shape. It determines the viscoelastic properties of solid materials based on tensile-compressional motion, which is governed by different equation of motion from RAR, besides the different boundary conditions. Even though such motion is within the continuum, it can be modeled as a lumped mass-spring system and can be assessed by measuring the overall strain or displacement of the sample in the vertical direction. Furthermore, the presence of a thin liquid layer/plug between the supporting surface and the bottom of the sample, greatly alleviating the requirement of a highly smooth surface of the sample, as the gravity will pull down the soft sample to be stably positioned on top of the thin liquid layer which provides a capillary adhesion to the sample. The tensile-compressive motion of the sample is largely 1D, thus TAR measurements are independent of the sample shape. As such, TAR is versatile, robust, and capable of analyzing a wide variety of samples, independent of the sample shape, as shown in our experimental measurements and theoretical framework. Interestingly, despite the differences in the physical principles underlining RAR and TAR, our results demonstrate consistent measurements of viscoelastic properties between the two techniques, underscoring the reliability and accuracy of both approaches.

4.2. Study limitations and validation of TAR measurements

The main goal of this study is to demonstrate the capability and operation principle of TAR as a new approach for viscoelastic characterization. Thus, our experiments with hydrogel samples and natural food samples focused on the measurements of their viscoelastic properties, with a limited scope in terms of investigating the mechanisms responsible for the changing viscoelastic properties of the cell-laden hydrogel constructs. We envision future studies will pursue these important objectives once TAR is established.

In addition, while it is worthwhile to validate TAR by comparing results with those using conventional techniques such as shear rheometry measurement of the same sample. However, since the underlying mechanisms of these techniques are distinctively different from TAR, direct comparison of results thus is challenging and may not be easily obtained as measurement conditions and parameters are not translatable. It is possible to compare TAR and RAR results of the same samples, as shown in the example in Fig. 2, but RAR is not optimized for testing of free-standing samples as the tensile-compression movement of the samples dominates the measured signals. Thus, RAR has a much lower signal to noise ratio in the free-standing samples. Furthermore, RAR

requires a circular shape to form clean resonant modes of surface waves.

Furthermore, although SWE is not a conventional method used for typical rheology measurements, SWE has been established as a non-contact measurement technique for tissue elasticity, thus providing a convenient and meaningful validation for our TAR measurements of modulus of the same samples in this study.

4.3. Limitations of TAR and considerations for dimensional scaling effects

In this study, we performed TAR experiments in samples of small volumes with a range of heights, which determined the frequency of the oscillatory tensile-compressive motion of the sample. Thus, the viscosity and modulus measured of the sample was related to this specific frequency. Even though it is theoretically possible to measure samples of the same materials but different heights to investigate the impact of frequency on the viscoelasticity, the range of frequency is limited by the heights that are attainable in practice. This limits the use of TAR for cases when extremely high strain rate measurements are desired.

Experiments in this study show that TAR was unable to reliably measure samples with thickness less than 0.3 mm. This limitation is partially related to the frequency of the detection ultrasound transducer used in our prototype system (7 MHz), which corresponds to a wavelength of 0.21 mm. Implementing a higher frequency detection system could overcome this limitation for thinner samples. For instance, a detection frequency of 10 MHz would yield a wavelength of 0.15 mm, making TAR feasible for measurement of thinner samples. However, the application of TAR for such thinner samples is also limited as the thickness approaches the thickness of the liquid plug between the sample and the supporting surface as well as the difficulty in generating tensile-compression motion of a thin sample.

The accuracy of TAR measurements can be compromised in samples with large cross section area but low stiffness, since 1D assumption is made for the tensile-compression motion in the lumped mass-spring model. Samples with small diameters, or **high aspect ratios** (thickness \gg diameter) will behave more closely as 1D objects, with **unidirectional deformation** primarily along the vertical axis. However, **larger samples have greater freedom to deform in multiple dimensions**, leading to multi-axial stress and strain distributions. This behavior reduces the accuracy of the mass-spring model for larger samples. Such **dimensional scaling effects are dependent on sample stiffness and represent an important area for future investigation to refine TAR's applicability and accuracy for various sample**

geometry and mechanical properties.

5. Conclusions

This study demonstrates the capability of TAR for the characterization of free-standing soft biomaterial samples in small volumes. By utilizing ultrasound-based excitation and detection approach, TAR offers a non-contact approach to quantify the viscoelastic properties of samples of various dimensions and shapes, providing a robust tool for longitudinal monitoring of samples under sterile conditions over time. These capabilities enable TAR for diverse laboratory and industrial applications.

CRedit authorship contribution statement

Weiping Li: Writing – original draft, Visualization, Validation, Formal analysis, Data curation. **Eric C. Hobson:** Methodology, Investigation, Formal analysis, Conceptualization. **Kiera Downey:** Writing – original draft, Formal analysis, Data curation. **Timothy L. Hall:** Supervision, Methodology, Formal analysis, Data curation. **Jan P. Stegemann:** Writing – review & editing, Supervision, Conceptualization. **Cheri X. Deng:** Writing – review & editing, Writing – original draft, Supervision, Resources, Project administration, Methodology, Investigation, Funding acquisition, Formal analysis, Conceptualization.

Declaration of generative AI and AI-assisted technologies in the writing process

No generative AI and AI-assisted technologies were used in the writing process.

Declaration of competing interest

The authors declare that they have no known competing financial interests or personal relationships that could have appeared to influence the work reported in this paper.

Acknowledgement

Author Kiera Downey was supported in part by National Science Foundation (Grant 2225568) for performing shear wave imaging experiments to provide independent verification of elasticity measurements.

Appendix A. Supplementary data

Supplementary data to this article can be found online at <https://doi.org/10.1016/j.biomaterials.2025.123325>.

Data availability

Data will be made available upon request.

References

- [1] B. Corominas-Murtra, N.I. Petridou, Viscoelastic networks: forming cells and tissues, *Front. Phys.* 9 (2021).
- [2] J. Bico, E. Reyssat, B. Roman, Elastocapillarity: when surface tension deforms elastic solids, *Annu. Rev. Fluid Mech.* 50 (2018) 629–659.
- [3] N. Nadermann, C.Y. Hui, A. Jagota, Solid surface tension measured by a liquid drop under a solid film, *Proc. Natl. Acad. Sci. U. S. A.* 110 (26) (2013) 10541–10545.
- [4] R.W. Style, A. Jagota, C.Y. Hui, E.R. Dufresne, Elastocapillarity: surface tension and the mechanics of soft solids, *Annu. Rev. Condens. Matter Phys.* 8 (2017) 99–118.
- [5] J.L. Drury, D.J. Mooney, Hydrogels for tissue engineering: scaffold design variables and applications, *Biomaterials* 24 (24) (2003) 4337–4351.
- [6] A.S. Hoffman, Hydrogels for biomedical applications, *Adv. Drug Deliv. Rev.* 64 (2012) 18–23.
- [7] P.A. Janmey, J.P. Winer, J.W. Weisel, Fibrin gels and their clinical and bioengineering applications, *J. R. Soc. Interface* 6 (30) (2009) 1–10.
- [8] M.P. Lutolf, J.A. Hubbell, Synthetic biomaterials as instructive extracellular microenvironments for morphogenesis in tissue engineering, *Nat. Biotechnol.* 23 (1) (2005) 47–55.
- [9] S.V. Murphy, A. Atala, 3D bioprinting of tissues and organs, *Nat. Biotechnol.* 32 (8) (2014) 773–785.
- [10] O. Chaudhuri, L. Gu, D. Klumpers, M. Darnell, S.A. Bencherif, J.C. Weaver, N. Huebsch, H.P. Lee, E. Lippens, G.N. Duda, D.J. Mooney, Hydrogels with tunable stress relaxation regulate stem cell fate and activity, *Nat. Mater.* 15 (3) (2016) 326–334.
- [11] J. Li, X. Jia, L. Yin, Hydrogel: diversity of structures and applications in food science, *Food Rev. Int.* 37 (3) (2021) 313–372.
- [12] E. Satchani Keneth, A. Kamyshny, M. Totaro, L. Beccai, S. Magdassi, 3D printing materials for soft robotics, *Adv. Mater.* 33 (19) (2021) e2003387.
- [13] O. Chaudhuri, L. Gu, M. Darnell, D. Klumpers, S.A. Bencherif, J.C. Weaver, N. Huebsch, D.J. Mooney, Substrate stress relaxation regulates cell spreading, *Nat. Commun.* 6 (2015) 6364.
- [14] A.J. Engler, S. Sen, H.L. Sweeney, D.E. Discher, Matrix elasticity directs stem cell lineage specification, *Cell* 126 (4) (2006) 677–689.
- [15] S.L. Rowe, S. Lee, J.P. Stegemann, Influence of thrombin concentration on the mechanical and morphological properties of cell-seeded fibrin hydrogels, *Acta Biomater.* 3 (1) (2007) 59–67.
- [16] M.L. Oyen, Mechanical characterisation of hydrogel materials, *Int. Mater. Rev.* 59 (1) (2013) 44–59.
- [17] C.J. Walker, D. Batan, C.T. Bishop, D. Ramirez, B.A. Aguado, M.E. Schroeder, C. Crocini, J. Schwisow, K. Moulton, L. Macdougall, R.M. Weiss, M.A. Allen, R. Dowell, L.A. Leinwand, K.S. Anseth, Extracellular matrix stiffness controls cardiac valve myofibroblast activation through epigenetic remodeling, *Bioeng Transl Med* 7 (3) (2022) e10394.
- [18] B.M. Richardson, C.J. Walker, M.M. Maples, M.A. Randolph, S.J. Bryant, K. S. Anseth, Mechanobiological interactions between dynamic compressive loading and viscoelasticity on chondrocytes in hydrazone covalent adaptable networks for cartilage tissue engineering, *Adv. Healthcare Mater.* 10 (9) (2021) e2002030.
- [19] R.S. Lakes, Viscoelastic measurement techniques, *Rev. Sci. Instrum.* 75 (4) (2004) 797–810.
- [20] P. Cicuta, A.M. Donald, Microrheology: a review of the method and applications, *Soft Matter* 3 (12) (2007) 1449–1455.
- [21] M. Daviran, J. Catalano, K.M. Schultz, Determining how human mesenchymal stem cells change their degradation strategy in response to microenvironmental stiffness, *Biomacromolecules* 21 (8) (2020) 3056–3068.
- [22] B.A. Juliar, M.T. Keating, Y.P. Kong, E.L. Botvinick, A.J. Putnam, Sprouting angiogenesis induces significant mechanical heterogeneities and ECM stiffening across length scales in fibrin hydrogels, *Biomaterials* 162 (2018) 99–108.
- [23] C.M. Ghajar, K.S. Blevins, C.C. Hughes, S.C. George, A.J. Putnam, Mesenchymal stem cells enhance angiogenesis in mechanically viable prevascularized tissues via early matrix metalloproteinase upregulation, *Tissue Eng.* 12 (10) (2006) 2875–2888.
- [24] P. Lambert, A. Chau, A. Delchambre, S. Régnier, Comparison between two capillary forces models, *Langmuir* 24 (7) (2008) 3157–3163.
- [25] S.F. Cheng, M.O. Robbins, Nanocapillary adhesion between parallel plates, *Langmuir* 32 (31) (2016) 7788–7795.
- [26] C. Cinbis, N.N. Mansour, B.T. Khuri-Yakub, Effect of surface tension on the acoustic radiation pressure-induced motion of the water–air interface, *J. Acoust. Soc. Am.* 94 (4) (1993) 2365–2372.
- [27] S.A. Elrod, B. Hadimioglu, B.T. Khuri-Yakub, E.G. Rawson, E. Richey, C.F. Quate, N.N. Mansour, T.S. Lundgren, Nozzleless droplet formation with focused acoustic beams, *J. Appl. Phys.* 65 (9) (1989) 3441–3447.
- [28] E.C. Hobson, W. Li, B.A. Juliar, A.J. Putnam, J.P. Stegemann, C.X. Deng, Resonant acoustic rheometry for non-contact characterization of viscoelastic biomaterials, *Biomaterials* 269 (2021) 120676.
- [29] S. Pansino, B. Taisne, Shear wave measurements of a Gelatin’s young’s modulus, *Front. Earth Sci.* 8 (2020).
- [30] E.C. Hobson, W. Li, N.E. Friend, A.J. Putnam, J.P. Stegemann, C.X. Deng, Crossover of surface waves and capillary-viscous-elastic transition in soft biomaterials detected by resonant acoustic rheometry, *Biomaterials* 302 (2023) 122282.
- [31] F. Monroy, Surface hydrodynamics of viscoelastic fluids and soft solids: surfing bulk rheology on capillary and Rayleigh waves, *Adv. Colloid Interface Sci.* 247 (2017) 4–22.
- [32] R.M.S. Sigrist, J. Liau, A.E. Kaffas, M.C. Chammas, J.K. Willmann, Ultrasound elastography: review of techniques and clinical applications, *Theranostics* 7 (5) (2017) 1303–1329.